

---

# Techniques for compact source extraction on CMB maps

R. B. Barreiro<sup>1</sup>

Instituto de Física de Cantabria, CSIC - Universidad de Cantabria, Avda. de los Castros s/n,  
39005 Santander, Spain  
[barreiro@ifca.unican.es](mailto:barreiro@ifca.unican.es)

The detection of compact sources embedded in a background is a very common problem in many fields of Astronomy. In these lecture notes we present a review of different techniques developed for the detection and extraction of compact sources, with a especial focus on their application to the field of the cosmic microwave background radiation. In particular, we will consider the detection of extragalactic point sources and the thermal and kinematic Sunyaev-Zeldovich effects from clusters of galaxies.

## 1 Introduction

Observations of an astrophysical signal in the sky are usually corrupted by some level of contamination (called *noise* or *background*), due to other astrophysical emissions and/or to the detector itself. A common situation is that the signals of interest are spatially well-localised, i.e. each of them covers only a small fraction of the image, but we do not know a priori its position and/or its amplitude. Some examples are the detection of extragalactic sources in cosmic microwave background (CMB) observations (see Fig. 1), the identification of local features (emission or absorption lines) in noisy one-dimensional spectra or the detection of objects in X-ray images. It is clear that our ability to extract all the useful information from the image will critically depend on our capacity to disentangle the signal(s) of interest from the background.

The process to detect a localised signal in a given image usually involves three different steps, which are not necessarily independent:

1.- Processing: some processing of the data (commonly linear filtering) is usually performed in order to amplify the searched signal over the background. This is an important step because in many cases the signals are relatively weak with respect to the background and it becomes very difficult to detect them in the original image. This is illustrated in Figure 2: the top panel shows a simulation of white noise where a source with a Gaussian profile has been

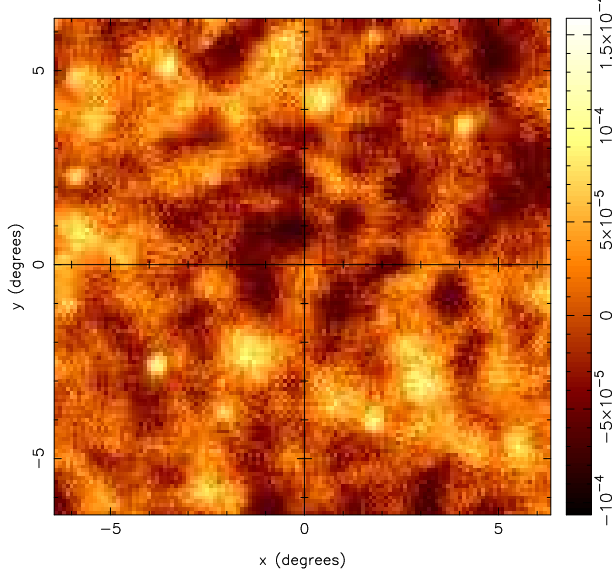


**Fig. 1.** Simulation of the 44 GHz Planck frequency channel in a small patch of the sky, containing CMB, Galactic foregrounds, extragalactic point sources and instrumental noise. The point sources can be seen as localised objects embedded in the background. The Planck Mission [69] is a satellite of the European Space Agency to be launched in 2007 that will provide with multifrequency observations of the whole sky with unprecedented resolution and sensitivity.

added in the centre of the map; the bottom panel gives the same simulation after filtering with the so-called matched filter. It becomes apparent that the source was hidden in the original image whereas it has been enhanced in the filtered image.

2.- Detection: we need a detection criterion, the *detector*, to decide if some structure in the image is actually a real signal or if it is due to the background. A very simple and widely used detector in Astronomy is *thresholding*: if the intensity of the image is above a given value (e.g.  $5\sigma$ , where  $\sigma$  is the dispersion of the map), a detection of the signal is accepted, otherwise one assumes that only background is present. In the example of Fig. 2, we see that several peaks appear in the filtered image (right panel) but only one of them is above the considered threshold  $\nu\sigma$ . Therefore, in this case, we would accept only the highest peak as a true signal. Note that thresholding uses only the intensity of the data to make the decision, however other useful information could also be included in order to improve the detector (e.g. curvature, size, etc.).

3.- Estimation: a procedure must be established to estimate the parameters (amplitude, size, position...) characterising the detected signal. For instance, a simple possibility is to estimate the required parameters by fitting the signal to its theoretical profile.

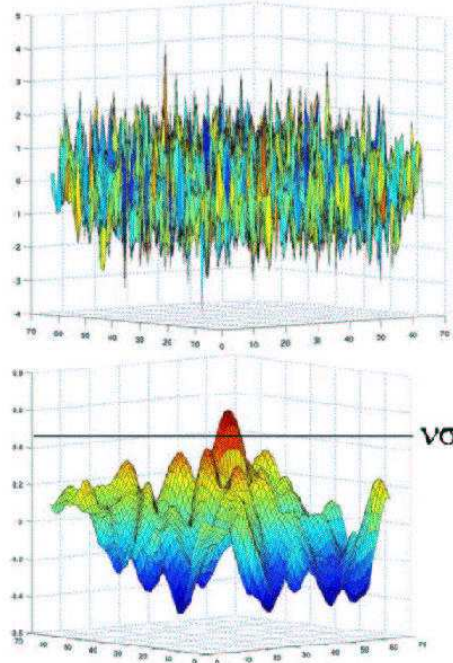


**Fig. 2.** This example illustrates the importance of filtering. A source with a Gaussian profile has been placed in the centre of the image in a background of white noise. The source can not be distinguished in the original image (left panel), however, after filtering (right panel), the source is enhanced over the background fluctuations.

The aim of these lecture notes is to present the problem of the extraction of localised signals (compact sources) in the context of CMB Astronomy and to review some of the methods developed to deal with it. In section 2, we outline the problem of component separation in CMB observations. Section 3 reviews some of the techniques developed for extraction of point sources, including, among others, the matched filter and the Mexican Hat Wavelet. Sections 4 and 5 deal with the extraction of the thermal and kinematic Sunyaev-Zeldovich effects in multifrequency microwave observations, respectively. Section 6 briefly discusses some techniques for the extraction of statistical information from undetected sources. Finally, in section 7 we present our conclusions.

## 2 The microwave sky and the problem of component separation

Microwave observations contain not only the cosmological signal but also Galactic foregrounds, thermal and kinetic Sunyev-Zeldovich (SZ) effects from clusters of galaxies and emission from extragalactic point sources [15, 83, 5, 11]. In addition, they also contain some level of noise coming from the detector itself. In order to recover all the wealth of information encoded in the CMB anisotropies, it is crucial to separate the cosmological signal from the rest of the components of the sky. Moreover, the foregrounds themselves contain very valuable information about astrophysical phenomena [28]. Therefore, the development of tools to reconstruct the different components of the microwave sky is of great interest, not only to clean the CMB signal but also to recover all the useful information present in the foregrounds.

The main Galactic foregrounds are the synchrotron, free-free and thermal dust emissions. The synchrotron emission is due to relativistic electrons accelerated in the Galactic magnetic field. The free-free emission is the thermal bremsstrahlung from hot electrons when accelerated by ions in the interstellar gas. The observed dust emission is the sum over the emission from each dust grain along the line of sight (dust grains in our galaxy are heated by the interstellar radiation field, absorbing UV and optical photons and re-emitting the energy in the far infrared). In addition, there is some controversial about the presence of an anomalous foreground at microwave frequencies [26, 66, 56, 37, 27] that could be due to the emission of spinning dust grains [33, 34].

The thermal SZ effect [78, 79] is a spectral distortion of the blackbody spectrum of the CMB produced by inverse Compton scattering of microwave photons by hot electrons in the intracluster gas of a cluster of galaxies. In addition, the radial peculiar velocities of clusters also produce secondary anisotropies in the CMB via the Doppler effect, known as the kinetic SZ effect [80]. For a review on the SZ effect, see [13].

The thermal SZ effect has a distinct spectral signature. It produces a temperature decrement below 217 GHz and an increment above that frequency. The change in intensity (see Fig. 3) is given by

$$\Delta I = \frac{2(kT_o)^3}{(hc)^2} \frac{x^4 e^x}{(e^x - 1)^2} y_c \left[ x \coth \frac{x}{2} - 4 \right] \quad , \quad x = \frac{h\nu}{kT_o} \quad (1)$$

where  $y_c \equiv \frac{k\sigma_T}{m_e} \int dl T_e n_e$  is the Compton parameter and is a function of the electron density  $n_e$  and temperature  $T_e$ . This distinct frequency dependence can be used in multifrequency observations to separate the thermal SZ effect from the rest of components of the microwave sky and, in particular, from the CMB.

The Doppler shift induced by the kinetic SZ effect in the CMB temperature fluctuations is given by:

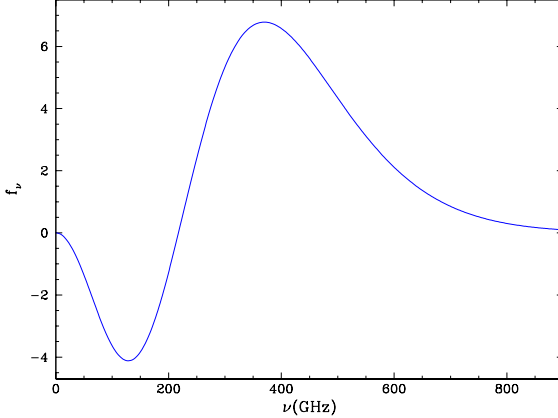


**Fig. 3.** Frequency dependence of the thermal SZ effect (in arbitrary units)

$$\frac{\Delta T}{T} = -\tau \frac{v_r}{c} \quad (2)$$

where  $v_r$  is the radial velocity of the cluster and  $\tau = \sigma_T \int n_e dl$  is the optical depth.

The thermal and kinetic SZ effects imprint anisotropies in the CMB at scales below a few arcminutes. Therefore, they are compact sources whose shape is given by the convolution of the beam of the experiment with the cluster profile. It is anticipated that will be very difficult to detect the kinetic SZ effect and to separate it from the cosmological signal. This is due to the fact that it has the same frequency dependence as the CMB (since it is just a Doppler shift). Moreover, it is a very weak effect, around one order of magnitude lower than the thermal effect. The SZ effect is a very useful cosmological probe. Future SZ surveys will allow one to obtain very valuable information about some of the cosmological parameters, such as  $H_0$ ,  $\Omega_m$ ,  $\Omega_\Lambda$  and  $\sigma_8$  (for a review see [17])

Emission from extragalactic point sources is an important contaminant for high-resolution CMB experiments. By *point source* is meant that the typical angular size of these objects is much smaller than the resolution of the experiment (which is usually the case in CMB observations) and therefore they appear in the data as point-like objects convolved with the beam of the instrument. There are two main source populations: radio sources, which dominate at lower frequencies ( $\lesssim 300$  GHz) and far-IR sources which give the main contribution at higher frequencies ( $\gtrsim 300$  GHz). These populations consist mainly of compact AGN, blazars and radio loud QSOs in the radio and of inactive spirals galaxies in the far-IR. Different models for the radio [85, 86, 29, 39] and infrared [41, 32, 40] point source populations have been proposed. However, there are still many uncertainties with regard to the number of counts

and the spectral behaviour of these objects, due to a lack of data at the frequency range explored by CMB experiments. Therefore experiments such as Planck will provide with unique information to understand the astrophysical processes taking place in these populations of sources. An additional problem is the heterogeneous nature of extragalactic point sources, since, among other complications, each source has its own frequency dependence. Therefore they can not be treated as a single foreground to be separated from the other components by means of multifrequency observations.

There are basically two different approaches to perform component separation. The first one tries to reconstruct simultaneously all the components of the microwave sky whereas the second one focuses in just one single component. The first type of methods include the Wiener filter [14, 81], maximum-entropy method [49, 50, 76, 11, 8, 77] and blind source separation [4, 62, 63, 25, 10, 68]. These methods usually assume that the components to be reconstructed can be factorised in a spatial template times a frequency dependence (but see [36] for a recent work where this assumption is not necessary). This assumption is correct for the CMB and the SZ effects but it is only an approximation for the Galactic foregrounds. In addition, point sources can not be factorised in this way and therefore these techniques are not well-suited for extracting this contaminant. Regarding the second approach, it consists on methods designed to extract a particular component of the sky. For instance, the blind EM algorithm of [65] or the internal linear combination of [11, 84, 35] try to recover only the CMB component. Moreover, this type of approach is especially useful for the detection of localised objects such as extragalactic point sources or the SZ effects. In these lectures we will describe some of these methods, that have been developed with the aim of extracting compact sources from microwave observations.

### 3 Techniques for extraction of point sources

The most common approach to detect point sources embedded in a background is probably linear filtering. A linearly filtered image  $w(x)$  is obtained as the convolution<sup>1</sup> of the data  $y(x)$  with the filter  $\psi(x)$ :

$$w(x) = \int y(u)\psi(x-u)du \quad (3)$$

Note that those parts of the data that resemble the shape of the filter will be enhanced in the filtered map. Therefore, the filter should have a similar profile to that of the sought signal. Equivalently, we can work in Fourier space:

$$w(x) = \int y(q)\psi(q)e^{-iqx}dq \quad (4)$$

---

<sup>1</sup>Strictly speaking, the filtered image can be written as a convolution provided the filter is linear and spatially homogeneous (see e.g. [46])

where  $f(q)$  denotes the Fourier transform of  $f$ . From the previous equation, we see that the filter favours certain Fourier modes of the data.

In principle, it is equivalent to perform the filtering in real or Fourier space. However, from the practical point of view, direct convolution is a very CPU-time consuming operation. Therefore, working in Fourier space, where a simple product is performed, is preferred.

Different linear filters have been proposed in the literature to detect point sources in CMB maps, including the matched filter [82], the Mexican hat wavelet [18, 87, 89], the scale adaptive filter [73, 44], the biparametric scale adaptive filter [59] or the adaptive top hat filter [20]. In addition, non-linear techniques have also been proposed, such as the Bayesian method of [51] or the non-linear fusion of [60, 61]. In the next subsections we give an overview of some of these techniques, including applications to CMB simulated data.

### 3.1 The matched filter

Let us assume that we have a signal of amplitude  $A$  at position  $x_0$  embedded in a background of dispersion  $\sigma$ . The amplification  $\mathcal{A}$  of the signal obtained with a filter is given by:

$$\mathcal{A} = \frac{w(x_0)/\sigma_w}{A/\sigma} \quad (5)$$

where  $w(x_0)$  is the value of the filtered map at the position of the source and  $\sigma_w$  is the dispersion of the filtered map. Therefore, if the amplification is greater than one, the contrast between the signal and the background has been increased in the filtered map, improving the chances of detecting the source with respect to the original data. This is the main idea behind filtering: it puts you in a better position to detect the sources.

The *matched filter* (MF) is defined as the linear filter that gives maximum amplification of the signal. As an example, we will outline how to construct the MF for a source  $s(x)$  with spherical symmetry (a more detailed derivation can be found e.g. in [46]). Let us consider a set of 2-dimensional data  $y(\mathbf{x})$ :

$$\begin{aligned} y(\mathbf{x}) &= s(x) + n(\mathbf{x}) \\ s(x) &= A\tau(x) \end{aligned} \quad (6)$$

where  $\mathbf{x}$  is a 2-dimensional vector of position and  $x = |\mathbf{x}|$ . The source is characterised by a (spherically symmetric) profile  $\tau(x)$  and an amplitude  $A = s(0)$ .  $n(\mathbf{x})$  is the noise (or background) contribution which, for simplicity, is assumed to be a homogeneous and isotropic random field with zero mean and characterised by a power spectrum  $P(q)$  ( $q = |\mathbf{q}|$ ), i.e.,

$$\langle n(\mathbf{q})n^*(\mathbf{q}') \rangle = P(q)\delta^2(\mathbf{q} - \mathbf{q}') \quad (7)$$

where  $n(\mathbf{q})$  is the 2-dimensional Fourier transform.

Let us introduce a filter  $\psi$  with spherical symmetry. The filtered field  $w$  is given by:

$$w(\mathbf{x}) = \int y(\mathbf{q})\psi(q)e^{-i\mathbf{q}\mathbf{x}}d\mathbf{q} \quad (8)$$

It can be shown that the filtered field at the position of the source (for simplicity we will assume that the source is at the origin) is given by:

$$w(\mathbf{0}) = 2\pi \int qs(q)\psi(q)dq, \quad (9)$$

whereas the variance of the filtered field is obtained as:

$$\sigma_w^2 = 2\pi \int qP(q)\psi^2(q)dq \quad (10)$$

We want to find the filter that satisfies the following two conditions:

1.  $\langle w(\mathbf{0}) \rangle = A$
2.  $\sigma_w^2$  is a minimum with respect to the filter  $\psi$

The first condition means that the filter is an unbiased estimator of the amplitude of the source and gives straightforwardly the constraint:

$$\int q\tau(q)\psi(q)dq = \frac{1}{2\pi} \quad (11)$$

In order to minimise the variance of the filtered map (condition 2) including the previous constraint, we introduce a Lagrange multiplier  $\lambda$ :

$$\mathcal{L}(\psi) = \sigma_w^2(\psi) + \lambda \left[ \int q\tau(q)\psi(q)dq - \frac{1}{2\pi} \right] \quad (12)$$

Taking variations with respect to  $\psi$  and setting the result equal to zero, we find the matched filter:

$$\psi(q) = k \frac{\tau(q)}{P(q)} \quad (13)$$

$$k = \left[ 2\pi \int q \frac{\tau^2(q)}{P(q)} dq \right]^{-1} \quad (14)$$

Note that the matched filter is favouring those modes where the contribution of the signal ( $\tau$ ) is large and that of the noise ( $P$ ) is small.

Assuming simple models for the Galactic foregrounds, [82] has given an estimation of the catalogue of point sources that Planck will produce. According to this work, the number of sources detected by Planck above a  $5\sigma$  level in a sky area of 8 sr will range from around 650 for the 70 GHz channel to around 38000 at 857 GHz.

The matched filter has also been applied for the detection of point sources in the 1st-year WMAP data [11]. Using this technique, a catalogue of 208 extragalactic point sources has been provided.

### 3.2 The Mexican Hat Wavelet

Wavelet techniques are very versatile tools that only recently have been applied to the analysis of CMB maps. The main property that makes wavelet transforms so useful is that they retain simultaneously information about the scale and position of the image. This means that we can study the structure of an image at different scales without loosing all the spatial information (as it occurs in the case of the Fourier transform). There is not a unique way to construct a wavelet transform (see e.g. [24, 16]). In this section we will focus on one particular wavelet, the Mexican Hat Wavelet (MHW), that has been successfully implemented for the detection of point sources with a Gaussian profile in CMB simulated observations [18, 87, 89]. The MHW is the second

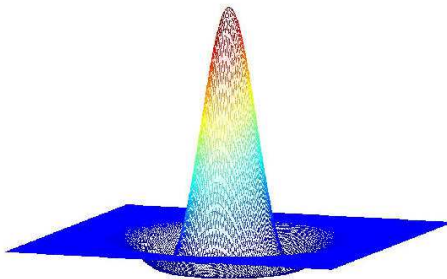


**Fig. 4.** The Mexican Hat Wavelet in 2 dimensions.

derivative of the Gaussian function (see Fig. 4):

$$\psi(x) = \frac{1}{\sqrt{2\pi}} \left[ 2 - \left( \frac{x}{R} \right)^2 \right] \exp \left( -\frac{x^2}{2R^2} \right) \quad (15)$$

and in Fourier space is given by:

$$\psi(q) \propto (qR)^2 \exp \left( -\frac{(qR)^2}{2} \right) \quad (16)$$

where  $R$  is the scale of the MHW, a parameter that determines the width of the wavelet. Note that  $\psi(x)$  – and wavelet functions in general – are compensated, i.e., the integral below the curve is zero. When filtering the data with the MHW, this property helps to remove contributions of the background with a scale of variation larger than the one of the wavelet.

The method to detect point sources is based on the study of the wavelet coefficients map (i.e. the image convolved with the MHW) at a given scale. Those wavelet coefficients above a fixed threshold are identified as point source candidates. The reason why this works well, it is because point sources are amplified in wavelet space. This can be easily seen in Fig. 5, which shows a graphical example of the performance of the MHW for a simulation of the Planck 857 GHz channel. Three of the panels correspond to the dust emission

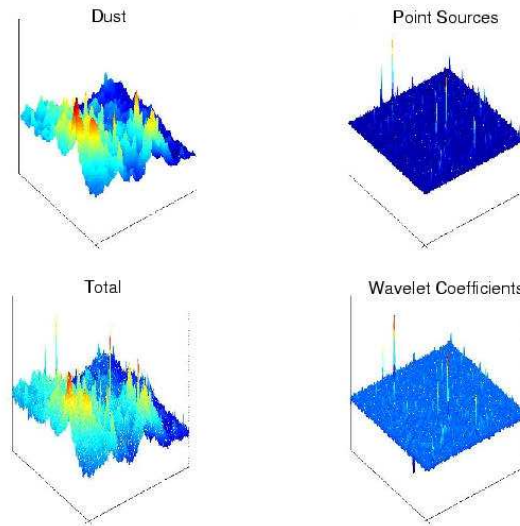


**Fig. 5.** An example of the performance of the MHW for a simulation of the Planck 857 GHz channel (see text for details).

(top-left), which is the dominant contaminant at this frequency, the emission of the extragalactic point sources (top-right) and the total emission at this frequency (bottom-left) including the Galactic foregrounds, CMB, SZ effect, extragalactic point sources and instrumental noise. The last panel (bottom-right) shows the total emission map after convolution with a MHW at a certain scale  $R_0$ . It is clear that in the wavelet coefficients map a large fraction of the background has been removed and that the signal of the point sources has been enhanced. Therefore, the detection level in wavelet space is greater than the detection level in real space:

$$\frac{\omega(R)}{\sigma_\omega(R)} > \frac{A}{\sigma} \quad (17)$$

where  $\omega(R)$  is the wavelet coefficient at scale  $R$  at the position of the source,  $\sigma_\omega$  is the dispersion of the wavelet coefficients map,  $A$  is the amplitude of the source and  $\sigma$  is the dispersion of the real map.

Note that the amplification (defined as the ratio between the detection level in wavelet space and the detection level in real space) depends on the wavelet scale  $R$ . In fact, for a given image, there exists an optimal scale  $R_0$  that gives maximum amplification for the point sources and that can be determined from the data. For a point source convolved with a Gaussian beam of dispersion  $\sigma_b$ , the value of the wavelet coefficient  $\omega(R)$  at the position of the source is given by

$$\omega(R) = 2R\sqrt{2\pi}A \frac{(R/\sigma_b)^2}{[1 + (R/\sigma_b)^2]^2} \quad (18)$$

whereas the dispersion of the wavelet coefficients map at scale  $R$  is

$$\sigma_\omega^2(R) = 2\pi R^2 \int P(q)|\psi(qR)|^2 q dq \quad (19)$$

where  $P(q)$  is the power spectrum of the background. Taking the previous expressions into account, one can obtain the optimal scale  $R_0$  by maximising the amplification  $\mathcal{A}$  versus  $R$ . Fig.6 shows the amplification of the signal versus the scale for simulated observations of the Planck Low and High Frequency Instruments (LFI and HFI). Note that the optimal scale is close to  $\sigma_b$ . This is expected, since this is the scale that characterises the source, but the value of  $R_0$  will also depend on the background. For instance, if the noise contribution is more important at scales smaller than the one of the source, this will tend to move the optimal scale to values greater than  $\sigma_b$  and vice versa. Although the MHW will produce, in general, slightly less amplification than the MF, it has the advantage of being an analytical function, which greatly simplifies the use of this technique.

The procedure to detect point sources is as follows. First, the optimal scale  $R_0$  is obtained and the data are filtered with a MHW of scale  $R_0$ . Those pixels  $k$  above a given threshold are identified as point sources. The amplitude of the detected sources is then estimated using a multiscale  $\chi^2$  fit for each pixel  $k$ :

$$\chi_k^2 = \sum_{i,j} (\omega_{i,k}^{th} - \omega_{i,k}^o)^t V_{ij}^{-1} (\omega_{j,k}^{th} - \omega_{j,k}^o) \quad (20)$$

where  $V$  is the covariance matrix between the different scales  $i, j$  and  $\omega_{i,k}^{th}$ ,  $\omega_{i,k}^o$  correspond, respectively, to the theoretical (given by equation 18) and observed wavelet coefficient at scale  $i$  and position  $k$ . Four scales are used for the  $\chi^2$ . Note that this fit can also be used to discard point source candidates: if a source candidate at pixel  $k$  does not have an acceptably low value of  $\chi^2$  could be rejected as a point source.

The MHW technique has been implemented to deal with simulated Planck observations in flat patches of the sky [87] and also on the whole sphere [89].

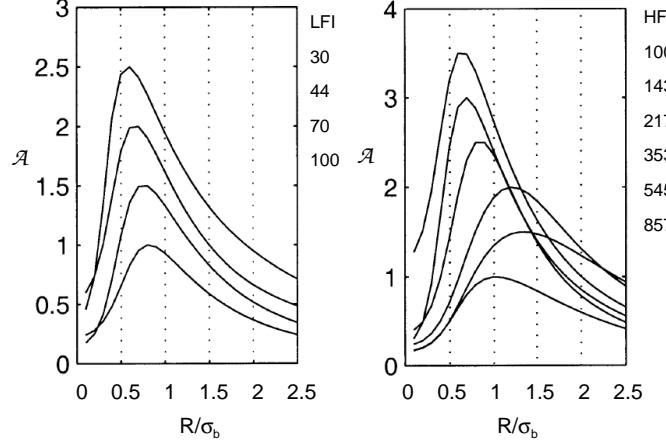


**Fig. 6.** Amplification (in arbitrary units) versus wavelet scale  $R$  (in units of the beam dispersion) for a typical region of the sky (the 100 GHz channel of the Low Frequency Instrument has been withdrawn from the final Planck payload due to financial shortage).

The procedure to detect point sources on spherical data is very similar to the one outlined before, but, in this case, the Spherical Mexican Hat Wavelet is used to convolve the data, which is given by [64]

$$\begin{aligned} \Psi_S(y, R) &= \frac{1}{\sqrt{2\pi}N(R)} \left[ 1 + \left(\frac{y}{2}\right)^2 \right]^2 \left[ 2 - \left(\frac{y}{R}\right)^2 \right] e^{-y^2/2R^2}, \\ N(R) &\equiv R \left( 1 + \frac{R^2}{2} + \frac{R^4}{4} \right)^{1/2}. \end{aligned} \quad (21)$$

$y$  is the distance to the tangent plane which is given by  $y \equiv 2 \tan \frac{\theta}{2}$ , where  $\theta$  is the latitude angle. Another important point when dealing with spherical data is the estimation of the optimal scale. In CMB observations, the contaminants can be very anisotropic in the sky. This means that the properties of the background change significantly for different areas of the sky and therefore the optimal scale for filtering with the SMHW has to be obtained locally. This is simply done by projecting small patches of the sky on a plane and obtaining the optimal scale for each of them. The maps are then convolved with SMHW of different scales and the detection is performed on the sphere but with the corresponding  $R_0$  for each patch.

Table 1 shows the catalogue predicted by [89] using simulated Planck observations of the whole sky. In addition to CMB and point sources, Galactic foregrounds, thermal SZ and instrumental noise were included in the simulations. Using the recovered catalogue, mean spectral indices can also be estimated with good accuracy. The SMHW has also been adapted to deal with realistic asymmetric beams as those expected for the Planck Mission.

**Table 1.** Predicted point source catalogue using the SMHW from simulated Planck observations. The point sources have been detected outside a Galactic cut that varies from channel to channel (from no cut at the lowest frequency channels up to a Galactic cut with  $b = 25$  degrees for 857 GHz). The different columns correspond to: Planck frequency channel, number of detections (above the minimum flux), minimum flux, mean error, mean bias, number of optimal scales needed for the algorithm and completeness of the catalogue above the minimum flux (see [89] for details).

Frequency (GHz)	Number	Min. Flux (Jy)	$\bar{E}(\%)$	$\bar{b}(\%)$	$N_{R_o}$	Completeness (%)
857	27257	0.48	17.7	-4.4	17	70
545	5201	0.49	18.7	4.0	15	75
353	4195	0.18	17.7	1.4	10	70
217	2935	0.12	17.0	-2.5	4	80
143	3444	0.13	17.5	-4.3	2	90
100	3342	0.16	16.3	-7.0	4	85
70	2172	0.24	17.1	-6.7	6	80
44	1987	0.25	16.4	-6.4	9	85
30	2907	0.21	18.7	1.2	7	85

It is also interesting to note that the MHW technique has been combined with the maximum-entropy method [88]. Using Planck simulated data it was shown that the joint method improved the quality of both the reconstruction of the diffuse components and the point source catalogue.

Finally, we would like to point out that the MHW has been used for the detection of objects in X-ray images [22, 23] and, more recently, in SCUBA [6, 53] and Boomerang data [21].

### 3.3 The Neyman-Pearson detector and the biparametric scale adaptive filter

As mentioned in section 1, filtering helps the detection process because it amplifies the sought signal over the background. However, whether we filter or not, we still need a detection criterion – the detector – to decide if a given signal belongs to the background or to a true source. In addition, the final performance of the filter will clearly depend on the choice of the detector. A criterion that has been extensively used in Astronomy is thresholding, i.e.,

those pixels of the data above a given value (e.g.  $5\sigma$ ) are identified as the signal. Thresholding has a number of advantages, including its simplicity and the fact that it has a precise meaning in the case of Gaussian backgrounds in the sense of controlling the probability of spurious detections. However, it only uses a limited part of the information contained in the data, the intensity, to perform decisions.

An example of detector – based on the Neyman-Pearson rule – that takes into account additional information has been recently proposed in [7, 57, 58] for 1-dimensional signals and [59] for the 2-dimensional case. The first step of the procedure is to identify maxima as point source candidates. To decide then whether the maxima are due to the presence of background on its own or to a combination of background plus source, a Neyman-Pearson detector is applied, which is given by (for 2-dimensional signals):

$$L(\nu, \kappa, \epsilon) \equiv \frac{n(\nu, \kappa, \epsilon)}{n_b(\nu, \kappa, \epsilon)} \geq L_* \quad (22)$$

where  $n_b(\nu, \kappa, \epsilon) d\mathbf{x} d\nu d\kappa d\epsilon$  is the expected number of maxima of the background in the intervals  $(\mathbf{x}, \mathbf{x}+d\mathbf{x})$ ,  $(\nu, \nu+d\nu)$ ,  $(\kappa, \kappa+d\kappa)$  and  $(\epsilon, \epsilon+d\epsilon)$ , whereas  $n(\nu, \kappa, \epsilon) d\mathbf{x} d\nu d\kappa d\epsilon$  corresponds to the same number in the presence of background plus source.  $\nu$ ,  $\kappa$  and  $\epsilon$  are the normalised intensity, normalised curvature and normalised shear of the field respectively, and  $\mathbf{x}$  is the spatial variable. For a homogeneous and isotropic Gaussian background and point sources with spherical symmetry, it can be shown that the previous detector is equivalent to [59]:

$$\varphi(\nu, \kappa) = a\nu + b\kappa \geq \varphi_* \quad (23)$$

where  $a$  and  $b$  are constants that depend on the properties of the background and the profile of the source, and  $\varphi_*$  is a constant that needs to be fixed. Therefore, if the considered maximum satisfies  $\varphi \geq \varphi_*$ , we decide that the signal is present, otherwise we consider that the maximum is due to the presence of only background.

Using this detector, [59] compares the performance of different filters. In order to do this,  $\varphi_*$  is fixed to produce the same number of spurious sources for all the filters and then the number of true detections are compared. In their study they consider the matched filter, the Mexican hat wavelet, the scale adaptive filter and the biparametric scale adaptive filter (BSAF). In addition, the scale of the filter is allowed to vary (similarly to what is done in the Mexican hat wavelet technique) through the introduction of a parameter  $\alpha$ . For the case of a background with a scale-free power spectrum ( $P(q) \propto q^{-\gamma}$ ) and a source with Gaussian profile, the BSAF is given by:

$$\psi_{BSAF}(q) = N(\alpha)z^\gamma e^{z^2/2}(1 + cz^2), \quad z \equiv q\alpha R \quad (24)$$

where  $c$  is a free parameter.  $\alpha$  and  $c$  are optimised in order to produce the maximum number of true detections given a fixed number of spurious detections. For  $c = 0$  and  $\alpha = 1$  the MF is recovered. Using this approach the

performance of the considered filters has been studied for the case of a Gaussian white noise background. The results predict that, in certain cases, the BSAF can obtain up to around 40 per cent more detections than the other filters. Although in CMB observations the background is not usually dominated by white noise, this case can also be of interest to detect point sources on CMB maps that have been previously processed using a component separation technique such as the maximum-entropy method [88]. In this case, the expected contribution of foregrounds and CMB is subtracted from each of the frequency maps, leaving basically the emission of extragalactic point sources and white noise (as well as some residuals). In this type of maps, the application of this technique could be useful. In any case, a test of the BSAF on realistic CMB simulations would be necessary to establish how well this approach would perform on real data.

### 3.4 Bayesian approach to discrete object detection

Many of the standard techniques for the detection of point sources are based on the design of linear filters. However, other methods – usually more complicated – are also possible. For instance, [51] has recently proposed a Bayesian approach for the detection of compact objects. The method is based on the evaluation of the (unnormalised) posterior distribution  $\overline{Pr}(\theta|D)$  for the parameters  $\theta$  that characterise the unknown objects (such as position, amplitude or size), given the observed data  $D$ . The unnormalised posterior probability is given in terms of the likelihood  $Pr(D|\theta)$  and the prior  $Pr(\theta)$  as:

$$\overline{Pr}(\theta|D) \equiv Pr(D|\theta)Pr(\theta) \quad (25)$$

Two different strategies are proposed for the detection of compact sources: an exact approach that tries to detect all the objects present in the data simultaneously and an iterative – much faster – approach (called McClean algorithm). In both cases an estimation of the parameters of the sources as well as their errors are provided. For both methods, a Markov-Chain Monte-Carlo technique is used to explore the parameter space characterising the objects.

As an illustration of the performance of the method, [51] studies the performance of both algorithms for a simple example that contains 8 discrete objects with a Gaussian profile embedded on a Gaussian white noise background. The test image has  $200 \times 200$  pixels and the signal-to-noise ratio of the objects ranges from 0.25 to 0.5. Using the exact method, where the number of objects is an additional parameter to be determined by the algorithm, all the objects are detected with no spurious detections. However two of the objects (which overlapped in the noiseless data) are identified as a single detection. The results show that the parameters have been estimated with reasonably good accuracy. Unfortunately, although this method seems to perform very well, it is also very computationally demanding, what can make it unfeasible in many realistic applications.

The iterative approach tries to detect the objects one-by-one. This significantly reduces the CPU-time necessary for the algorithm whereas provides a convenient approximation to the exact method. For the simple example previously considered, the McClean algorithm provides quite similar results to the exact approach, with only one less object detected than the exact approach.

This approach is certainly very promising and can be very useful for the detection of compact sources in future CMB data. However it assumes the knowledge of the functional form of the likelihood, the prior of the parameters and the profile of the objects, which will not be known in many realistic situations. In addition, the presence of anisotropic contaminants (such as instrumental noise or Galactic foregrounds) would introduce additional complexity that would make the algorithm more computationally demanding. [51] gives some hints on how to deal with some of these problems. In any case, it would be very useful to test the performance of the method under realistic conditions in order to establish the real potentiality of the technique.

#### 4 Techniques for extraction of the thermal SZ effect

Another important application of the compact source extraction techniques is the detection of the thermal SZ effect due to galaxy clusters in microwave observations. The resolution of most CMB experiments (e.g. 5 arcminutes for the best Planck channels) is usually not enough to resolve the structure of the clusters of galaxies. Thus, the SZ emission appears in the CMB maps as compact sources whose shape is given by the convolution of the beam of the experiment with the profile of cluster. This means that most of the techniques used for the detection of extragalactic point sources could be easily adapted to detect the SZ effect (in one single map), just by including the correct profile of the sought source in the algorithm. This type of studies have been done for instance for the SAF [45], the MF [75] or the Bayesian approach [51] discussed in the previous section.

However, the thermal SZ effect has a very characteristic frequency signature that can be used to extract this emission, provided that multifrequency observations are available. One alternative to recover the SZ emission is to apply a component separation technique – such as the maximum-entropy method, Wiener filter or blind source separation – that tries to recover simultaneously all the different emissions of the microwave sky. The second possibility is to design specific methods to extract the SZ signal that make use of the multifrequency information [43, 30, 71]. Regarding this second strategy, we will describe two of the methods that have been devised for the extraction of the thermal SZ effect from multifrequency CMB observations. Both methods have been tested using Planck simulated data.

#### 4.1 Filtering techniques

[43] presents different filtering techniques for the detection of SZ clusters in multifrequency maps. Two alternative strategies are proposed: a combination technique and the design of a multifrequency filter (or multifilter). In both cases, the spatial profile of the clusters are assumed to be known. In the combination method, the individual frequency maps are linearly combined in an optimal way. The weights of the linear combination can be determined from the data and they are optimal in the sense of giving the maximum amplification of objects that have the required spatial profile and the correct frequency dependence. This combined map is then filtered either with the MF or with the SAF constructed taking into account the characteristics of this new map. In the second approach, each frequency map is filtered separately but the filters are constructed taking into account the cross-correlations between frequency channels as well as the spectral dependence of the SZ effect. Then, the filtered maps are added together. This second method can also be implemented for two different kind of filters: the matched multifilter and the scale-adaptive multifilter. [43] performs a comparison of all these techniques finding that the matched multifilter provides the best results. Another interesting point is that the combination method is appreciably faster than the multifilter technique, whereas it still detects a large fraction of the clusters found by the matched multifilter.

Taking these results into account, we will discuss in more detail the matched multifilter (MMF) approach<sup>2</sup>. Let us consider a set of  $N$  observed maps given by:

$$y_\nu(\mathbf{x}) = f_\nu A \tau_\nu(\mathbf{x}) + n_\nu(\mathbf{x}), \quad \nu = 1, \dots, N \quad (26)$$

where, for illustration purposes, it is assumed that the SZ signal is due to the presence of a single cluster located in the origin of the image. The first term of the right hand side describes the contribution of the sought signal (the thermal SZ effect in this case) whereas  $n_\nu$  is a generalised noise term that includes the sum of all the other components present in the map.  $f_\nu$  is the frequency dependence of the thermal SZ effect (normalised to be 1 at a reference frequency),  $\tau_\nu$  is the shape of the cluster at each frequency (i.e. the profile of the cluster convolved with the corresponding antenna beam) and  $A$  is the amplitude of the SZ effect at the reference frequency. For simplicity the profile of the cluster is assumed to be spherically symmetric and is parameterised by a characteristic scale – the core radius  $r_c$  – but a generalisation to more complex profiles can be easily done. The background is assumed to be a homogeneous and isotropic random field with zero mean value and cross-power spectrum  $P_{\nu_1 \nu_2}(q)$  defined as

$$\langle n_{\nu_1}(\mathbf{q}) n_{\nu_2}^*(\mathbf{q}') \rangle = P_{\nu_1 \nu_2}(q) \delta_D^2(\mathbf{q} - \mathbf{q}'), \quad q \equiv |\mathbf{q}| \quad (27)$$

---

<sup>2</sup>A similar technique has also been independently developed by [67], but in the context of the detection of extragalactic point sources in multifrequency observations

where  $n_\nu(\mathbf{q})$  is the Fourier transform of  $n_\nu(\mathbf{x})$  and  $\delta_D^2$  is the 2-dimensional Dirac distribution.

The MMF is given (in matrix notation) by

$$\mathbf{\Upsilon}(q) = \alpha \mathbf{P}^{-1} F, \quad \alpha^{-1} = \int d\mathbf{q} F^t \mathbf{P}^{-1} F \quad (28)$$

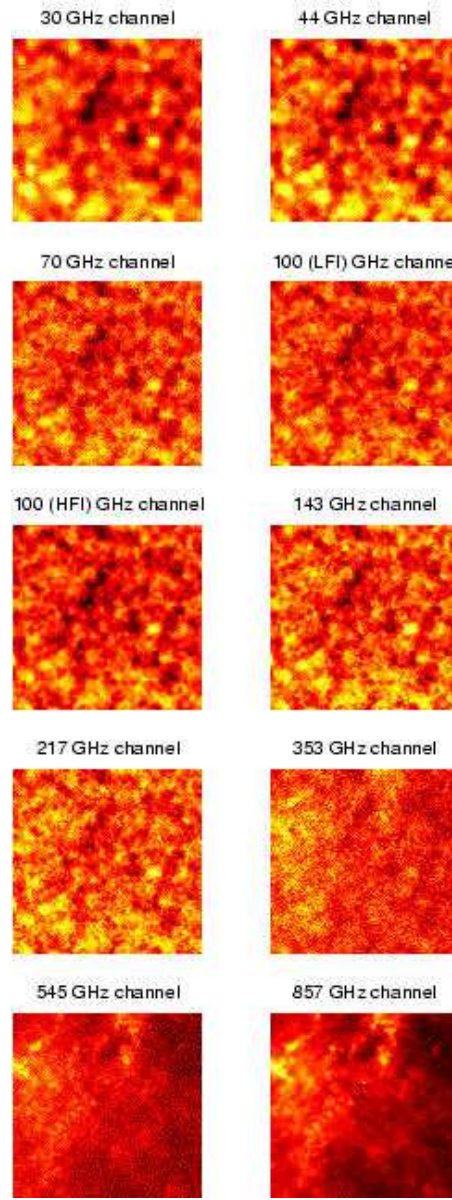
where  $F$  is the column vector  $F = [f_\nu \tau_\nu]$  and  $\mathbf{P}^{-1}$  is the inverse of the cross-power spectrum matrix  $P \equiv [P_{\nu_1 \nu_2}]$ .

The output map, where the detection of the SZ effect is finally performed, is obtained by filtering each frequency map with its corresponding filter  $\psi_\nu$  and then adding together all the filtered maps. The detection is then performed by looking for regions (5 or more pixels) of connected pixels above a  $3\sigma$  threshold. The maximum of the region determines the position of the cluster. In addition, the MMF is constructed so that the value of the intensity of the output map in the position of the source is an unbiased estimator of the amplitude. Therefore, the estimated amplitude of the SZ is simply given by the value of the output field in the considered maximum. Another interesting point is that the scale of the clusters  $r_c$  will not be known a priori. To overcome this problem, the data is multifiltered using different values of  $r_c$ . When the scale of the cluster coincides with that of the filter, the amplification of the signal will be maximum and that gives an estimation of the core radius  $r_c$ .

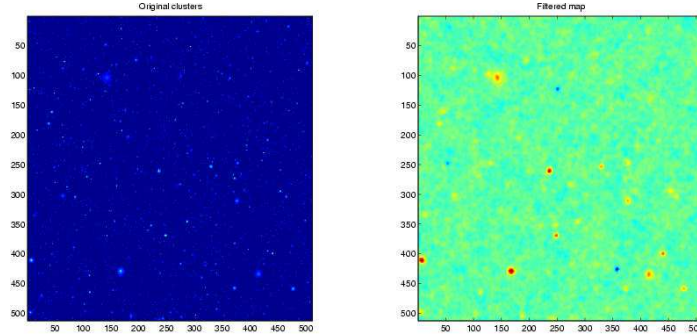
The MMF has been tested on Planck simulated data of small patches ( $12.8^\circ \times 12.8^\circ$ ) of the sky containing CMB, thermal and kinetic SZ effects, Galactic foregrounds (synchrotron, free-free, thermal dust and spinning dust) extragalactic point sources and instrumental noise. The simulated Planck data are shown in Fig. 7. Note that the SZ emission of clusters is completely masked by the rest of the components present in the data.

Fig. 8 shows the input thermal SZ emission included in the simulations and the reconstructed SZ map after filtering the data with a MMF of  $r_c=1$  pixel. Clusters with scales similar to the chosen one are clearly visible in the output map. [43] finds that the mean error in the determination of the position of the clusters is around 1 pixel whereas the core radii are determined with an error of 0.30 pixels. Regarding the determination of the cluster amplitudes, the mean error is around 30 per cent for the brightest clusters, whereas there is a bias in the estimation of the weakest clusters. This bias can be understood since most weak clusters will only reach the detection threshold if they are on top of a positive fluctuation of the background, which will lead to an overestimate of the amplitude. The bias could be reduced by improving the method of amplitude estimation (for instance by performing a fit to the profile of the cluster) that was simply given by the value of the maximum of the detection. Using this technique it is expected that Planck detects around 10000 clusters in 2/3 of the sky.

An extension of the multifilter technique to spherical data has been carried out by [74]. They test the method on realistic simulations of Planck in the whole sky that, in addition to the main microwave components, also include



**Fig. 7.** Simulated Planck channels used to test the performance of the MMF.



**Fig. 8.** The input (left panel) and reconstructed (right panel) SZ effect after filtering the data with a MMF of  $r_c = 1$  pixel.

the effect of non-uniform noise, sub-millimetric emission from celestial bodies of the Solar system and Galactic CO-line radiation. It is again found that the multifilter approach can significantly reduce the background, allowing the cluster signal to be detected.

#### 4.2 Bayesian non-parametric technique

[30] proposes an alternative method to detect SZ clusters in Planck data. The method has been also tested on the simulated data set of Fig. 7. The procedure is as follows. First of all, the frequency maps are significantly cleaned from the most damaging contaminants. In particular, extragalactic point sources are subtracted with the MHW and subsequently the emission from dust and CMB is removed using the information of the 857 and 217 GHz channels respectively. The next step consists on obtaining a map of the Compton parameter  $y_c$  in Fourier space by maximising, mode by mode, the posterior probability  $P(y_c|d)$ . Taking into account Bayes' theorem, this probability is given by

$$P(y_c|d) \propto P(d|y_c)P(y_c) \quad (29)$$

In order to perform this maximisation we need to know the likelihood function  $P(d|y_c)$  and the prior  $P(y_c)$ . Since the residuals left in the frequency maps are mainly dominated by the instrumental noise, the likelihood can be well approximated by a multivariate Gaussian distribution. In addition, one needs to assume a form for the prior  $P(y_c)$ . Using SZ simulations, [30] finds that the prior follows approximately the form  $P(y_c) \propto \exp(-|y_c|^2/P_{y_c})$  at each  $k$ -mode, where  $P_{y_c}$  is the power spectrum of the SZ map. Taking these results into account one gets, after maximising the posterior probability, the following solution for the  $y_c$  map at each mode:

$$y_c = \frac{\mathbf{d}\mathbf{C}^{-1}\mathbf{R}^\dagger}{\mathbf{R}\mathbf{C}^{-1}\mathbf{R}^\dagger + P_{y_c}^{-1}} \quad (30)$$

where  $d$  is the data,  $R$  is the response vector (that includes the information from the beam at each frequency and the frequency dependence of thermal SZ effect) and  $C$  is the cross-correlation matrix of the residuals. This result coincides with the multifrequency Wiener filter solution for the Compton  $y_c$  parameter. Note that the recovered  $y_c$  map will depend on the assumed power spectrum  $P_{y_c}$ . However, [30] shows that the final results do not depend significantly on the particular choice of  $P(y_c)$ , provided its form satisfies some general conditions. We would like to remark that this method does not need to make any assumption about the profile of the SZ clusters.

The recovered  $y_c$  map after applying this approach to the Planck simulated data of Fig. 7 is shown in Fig. 9. The detection and the estimation of the flux of

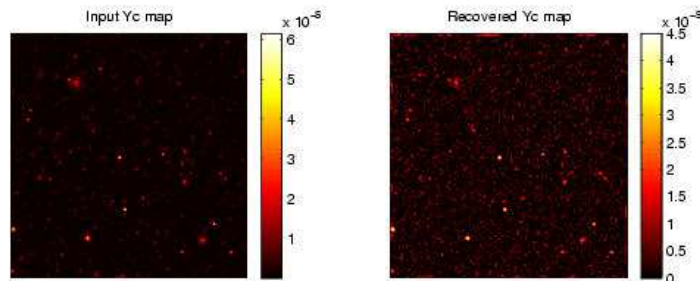


**Fig. 9.** The input (left panel) and reconstructed (right panel) Compton parameter map after applying the Bayesian non-parametric method.

clusters is performed in the recovered map using the package SExtractor [12], which selects connected pixels above a given threshold. Using a  $3\sigma$  threshold, this method predicts that Planck will detect around 9000 SZ clusters over 4/5 of the sky. In addition, it is shown that the flux of the clusters is estimated with no significant bias, which is important to carry out cosmological studies with the recovered catalogue.

## 5 Techniques for extraction of the kinetic SZ effect

The determination of peculiar velocities of individual clusters through the kinetic SZ effect is a very challenging task. This is mainly due to the facts that the kinetic SZ emission is very weak – around 1 order of magnitude weaker than the thermal SZ effect – and that it has the same frequency dependence as the CMB, meaning that both signals can not be separated using only multifrequency information. In addition, the presence of all the other components of the microwave sky and the instrumental noise makes even more difficult to detect this tiny signal. On the other side, we should take advantage of some characteristics of the kinetic SZ that could help to extract this emission. An

important point is to use the available information about the thermal SZ. Since both SZ effects are produced by clusters of galaxies, there is a strong spatial correlation between them. Multifrequency observations are also important to separate the kinetic SZ signal from the components of the microwave sky (except from the CMB). In particular, it is useful to consider observations at the frequency of 217 GHz, where the contribution of the thermal SZ is expected to be negligible. Finally, the probability distribution of the kinetic SZ signal (expected to be highly non-Gaussian) and its power spectrum are very different from the ones of the cosmological signal, what could also be used to separate it from the CMB fluctuations.

Due to the complexity of the problem, only a few methods have been proposed and tested with the aim of extracting this emission from microwave observations. For instance, [42] studied the performance of an optimal filter (which is actually a matched filter for the cluster profile) to detect the kinetic SZ effect, concluding that peculiar velocities could be measured only for a few fast moving clusters at intermediate redshift. [51] also applied their Bayesian algorithm to detect the kinetic SZ effect on CMB simulations at 217 GHz, but including only CMB and instrumental noise in the background. They claim that their technique is around twice as sensitive as the optimal linear filter. An alternative approach has been proposed by [38], which makes use of spatial correlation between the thermal and kinetic SZ effects. The method is tested in ideal conditions, using as starting point a map of the Compton parameter and a second map containing only CMB and kinetic SZ emission. In these ideal conditions the method provides very promising results. However, a detailed study of the performance of the method under realistic conditions should be done before establishing the true potentiality of this approach. Recently, [48] tested a modification of the matched multifilter on Planck simulated data for the detection of the kinetic SZ effect, that we discuss here in more detail.

### 5.1 The unbiased matched multifilter

If multifrequency information is available, we can also construct a MMF adapted to the kinetic SZ emission. As for the thermal SZ, the shape of the sought source will be the convolution of the antenna beam with the cluster profile but the frequency dependence will now follow that of the kinetic SZ emission. However, [48] found that the estimation of the kinetic SZ effect (and in fact that of the thermal SZ effect) using the MMF is intrinsically biased. It can be shown that this is due to the presence of two signals (the thermal and kinematic SZ effects in this case) that have basically the same spatial profile. Given the difference in amplitude of both effects, this bias is negligible for the case of the thermal SZ but it can be very important for the kinetic one. In order to correct this bias, a new family of filters, the unbiased matched multifilter (UMMF) has been constructed. For the case of the kinetic SZ effect, the UMMF is given by [48]:

$$\begin{aligned}\Phi &= \frac{1}{\alpha\gamma - \beta^2}(-\beta\mathbf{F} + \alpha\boldsymbol{\tau}) \\ \beta &= \int d\mathbf{q}\boldsymbol{\tau}^t\mathbf{P}^{-1}\mathbf{F}, \quad \gamma = \int d\mathbf{q}\boldsymbol{\tau}^t\mathbf{P}^{-1}\boldsymbol{\tau}\end{aligned}\quad (31)$$

These new multifilter leads to a slightly lower amplification of the sources than the MMF, but is intrinsically unbiased. The UMMF has been tested using Planck simulated data of small patches of the sky including CMB, Galactic foregrounds (synchrotron, free-free, thermal and spinning dust) and point sources. In order to test just the effect of the intrinsic bias on the estimation of the amplitude, simplistic simulations of clusters have been used, and the knowledge of the profile and position of the clusters has been assumed.

Fig. 10 shows the normalised histogram of the recovered parameter  $V = (v_r m_e c)/(k_B T_e)$  using the MMF and the UMMF obtained from simulations that contained clusters with  $r_c = 1.5$  arcmin,  $y_c = 10^{-4}$  and  $V = -0.1$ . For a temperature of the electrons of  $T_e \simeq 5$  keV, this value of  $V$  corresponds to a radial velocity along the line of sight of  $v_r \simeq 300$  kms $^{-1}$ . As predicted, the estimation of the amplitude of the kinetic SZ effect is strongly biased when using the MMF. However, this bias is corrected when the data are filtered with the UMMF. [48] also shows that this result remains valid for smaller values of  $y_c$  or  $V$ . Unfortunately, the error in the determination of peculiar velocities remains very large even for bright clusters. For instance, for  $y_c = 10^{-4}$  and  $T_e \simeq 5$  keV the statistical error in the determination of  $v_r$  is  $\sim 800$  kms $^{-1}$ . This means that Planck will not be able to measure, in general, the peculiar velocities of individual clusters, at least using just UMMF. Nonetheless, since the UMMF provides an unbiased estimation of  $v_r$ , it could be possible to measure mean peculiar velocities on large scales by averaging over many clusters.

## 6 Extraction of statistical information from undetected sources

In some cases the sought signal may be too weak to be individually detected or we may have found the brightest sources but we are unable to go down in flux. However, in this case, it may still be possible to extract some valuable statistical information from the background of sources. In this section we briefly discuss some works that have pursued this objective.

The differential number counts of extragalactic point sources are usually parameterised as

$$n(S) = kS^{-\eta}, \quad S > 0 \quad (32)$$

where  $S$  is the flux of the source and  $k$  and  $\eta$  are the normalisation and slope parameters respectively. [70] uses the information of the high order moments of simulated data containing CMB, noise and residual point sources, to estimate these two parameters. [47] determines  $k$  and  $\eta$  by fitting the characteristic

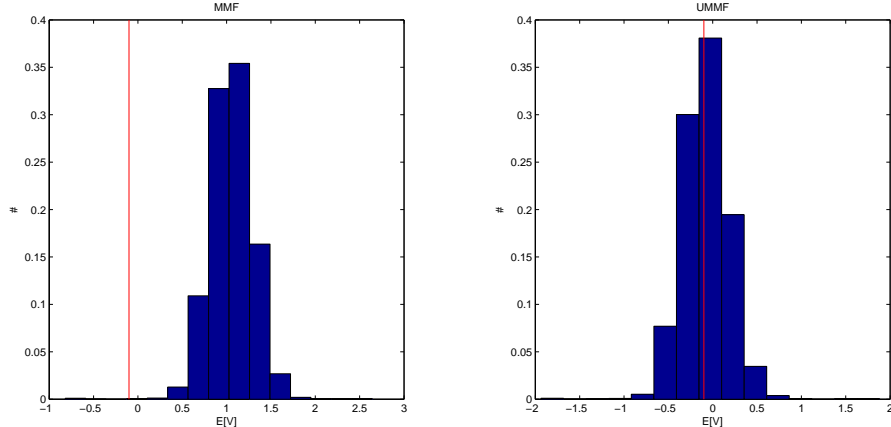


**Fig. 10.** Normalised histogram of the  $V$  parameter using the MMF (left panel) and the UMMF (right panel). The red vertical line indicates the input value of  $V$ .

function of the point sources distribution to an  $\alpha$ -stable model. The method is tested in the presence of a Gaussian background. These approaches offer interesting possibilities for the extraction of statistical information from an unresolved background of point sources. However, the study of their performance on more realistic conditions – that take into account, for instance, the presence of anisotropic noise and non-Gaussian foregrounds – remains to be done.

Another interesting possibility is the study of the bispectrum of undetected point sources since this quantity will depend on the characteristics of the underlying population of extragalactic point sources [54, 2]. It also provides with an estimation of the level of the contamination introduced by the residual point sources. In particular, [55] estimated the power spectrum of residual point sources in the WMAP data through the measurement of the bispectrum.

One may also use statistical information of the unresolved sources to identify which type of emission is present. In particular, [72] presents a detailed study of the contribution of the thermal SZ emission and of the extragalactic point sources to the probability distribution of the brightness map. The different imprints left by these two emissions would allow one to discriminate whether the excess of power found at small scales in some CMB data is due to an unresolved background of point sources or to the presence of unresolved SZ clusters. An alternative study based on the analysis of the Gaussianity of the wavelet coefficients has also been carried out to explain this excess of power [31].

Regarding the kinetic SZ effect, we have already mentioned that the detection of peculiar velocities of individual clusters will be a very challenging task. However, one could infer bulk flows on large scales what would provide

valuable cosmological information. This point has been addressed by different authors, including [52, 1, 3].

## 7 Conclusions

The development of techniques for the extraction of compact sources in CMB observations has become a very relevant and active topic. This is due to the necessity of cleaning the CMB maps from astrophysical contaminants that would impair our ability to extract all the valuable information encoded in the cosmological signal but also because the recovered catalogues of point sources and/or SZ clusters would contain themselves extremely relevant astrophysical and cosmological information.

An important effort has been done in the last years towards the development of more powerful and sophisticated tools to extract compact sources. Many of them have been tested on simulated Planck observations, showing their potentiality. However some important work still remains to be done. First of all, in some cases, quite ideal conditions have been assumed. For instance, it is commonly assumed that the cluster profile is known but, in general, this will not be the case for real data. Other methods have been applied to simulations that do not include foreground emissions. Therefore, these and other problematics – beam asymmetry, extension to the sphere, relativistic effects, anisotropic noise, etc. – present on real data should be taken into account to establish the true performance of the developed methods. Also, the methods do not always use all the available information present in the data. For instance, if multifrequency observations are available, it would be useful to include this multifrequency information in the detection of extragalactic point sources even if they do not follow a simple well-known spectral law. The final and most important step would be to apply these techniques to real CMB data (e.g. WMAP) as they become available.

We would also like to point out that many polarisation experiments are currently planned (or already operating) which will provide with a wealth of information about our universe [19]. Given the weakness of the cosmological signal in polarisation and the current lack of knowledge regarding the foreground emissions, a careful process of cleaning of the CMB polarisation maps is even more critical than for the intensity case. However no techniques have been yet specifically developed to extract compact sources from polarisation CMB observations. Therefore it is crucial to extend some of the current methods – or to develop new ones – to deal with this type of maps.

Finally, a very critical issue is to assess which is the impact of possible residuals left in the CMB data after applying these techniques [9]. In particular, it is very important to control the effect of undetected sources, or even possible artifacts introduced in the image after subtracting the signals, on the estimation of the power spectrum of the CMB. In addition, this process should not modify the underlying CMB temperature distribution, since

it would impair our ability to perform Gaussianity analyses of the CMB (or even lead us to wrong conclusions), which are of great importance to learn about the structure formation of our universe.

## Acknowledgements

RBB acknowledges the Universidad de Cantabria and the Ministerio de Educación y Ciencia for a Ramón y Cajal contract and J.M. Diego, D. Herranz, M. López-Caniego, E. Martínez-González, J.L. Sanz and P. Vielva for their help in the elaboration of these lecture notes. I would also like to thank the organisers for inviting me to participate in a very fruitful and interesting school.

## References

1. N. Aghanim, K. M. Górski, J.-L. Puget: *A&A*, **374**, 1 (2001)
2. F. Argüeso, J. González-Nuevo, L. Toffolatti: *ApJ*, **598**, 86 (2003)
3. F. Atrio-Barandela, A. Kashlinsky, J. P. Mücket: *ApJ*, **601**, 111 (2004)
4. C. Baccigalupi, L. Bedini, C. Burigana, G. De Zotti, A. Farusi, D. Maino, M. Maris, F. Perrotta, E. Salerno, L. Toffolatti, A. Tonazzini: *MNRAS*, **318**, 769 (2000)
5. A. J. Banday, C. Dickinson, R. D. Davies, R. J. Davis, K. M. Górski: *MNRAS*, **345**, 897 (2003)
6. V. E. Barnard, P. Vielva, D. P. I. Pierce-Price, A. W. Blain, R. B. Barreiro, J. S. Richer, C. Qualtrough: *MNRAS*, **352**, 961 (2004)
7. R. B. Barreiro, J. L. Sanz, D. Herranz, E. Martínez-González: *MNRAS*, **342**, 119 (2003)
8. R. B. Barreiro, M. P. Hobson, A. J. Banday, A. N. Lasenby, V. Stolyarov, P. Vielva, K. M. Górski: *MNRAS*, **351**, 515 (2004)
9. R. B. Barreiro, E. Martínez-González, P. Vielva, M. P. Hobson: *MNRAS*, submitted, preprint (astro-ph/0503039)
10. L. Bedini, D. Herranz, E. Salerno, C. Baccigalupi, E. E. Kuruoglu, A. Tonazzini: EURASIP Journal on Applied Signal Processing (Special Issue on Applications of Signal Processing in Astrophysics and Cosmology), **15**, 2400 (2005)
11. C. L. Bennett et al.: *ApJS*, **148**, 97 (2003)
12. E. Bertin, S. Arnouts: *A&AS*, **117**, 393 (1996)
13. M. Birkinshaw: *PhR*, **310**, 97 (1999)
14. F. R. Bouchet, R. Gispert, J. L. Puget: The MM/SUB-MM foregrounds and future CMB space missions. In: *The COBE workshop: Unveiling the cosmic infrared background* AIP Conference Proceedings, vol 348, ed by E. Dwek (1996), pp 255 – 270
15. F. R. Bouchet, R. Gispert: *New Astr.*, **4**, 443 (1999)
16. C. S. Burrus, R. A. Gopinath, H. Guo: *Introduction to Wavelets and Wavelet Transforms. A primer* (Prentice-Hall, Upper Saddle River, New Jersey 1998)
17. J. E. Carlstrom, G. P. Holder, E. D. Reese: *AR&A&A*, **40**, 643 (2002)

18. L. Cayón, J.L. Sanz, R.B. Barreiro, E. Martínez-González, P. Vielva, L. Toffolatti, J. Silk, J.M. Diego, F. Argüeso: MNRAS, **315**, 757 (2000)
19. A. Challinor: *Cosmic microwave background polarization analysis*, in this volume
20. L.-Y. Chiang, H. E. Jorgensen, I. P. Naselsky, P. D. Naselsky, I. D. Novikov, P. R. Christensen: MNRAS, **335**, 1054 (2002)
21. K. Coble et al., ApJS, submitted, preprint (astro-ph/0301599)
22. F. Damiani, A. Maggio, G. Micela, S. Sciortino: ApJ, **483**, 350 (1997)
23. F. Damiani, A. Maggio, G. Micela, S. Sciortino: ApJ, **483**, 370 (1997)
24. I. Daubechies: *Ten Lectures on Wavelets* (S.I.A.M., Philadelphia, 1992)
25. J. Dellabrouille, J. F. Cardoso, G. Patanchon: MNRAS, **346**, 1089 (2003)
26. A. de Oliveira-Costa et al.: ApJ, **567**, 363 (2002)
27. A. de Oliveira-Costa et al., M. Tegmark, R. D. Davies, C. M. Gutiérrez, A. N. Lasenby, R. Rebolo, R. A. Watson: ApJ, **606**, L89 (2004)
28. G. de Zotti, L. Toffolatti, F. Argüeso, R. D. Davies, P. Mazzotta, R. B. Partridge, G. F. Smoot, N. Vittorio: The Planck Surveyor Mission: Astrophysical Prospects. In *3K Cosmology, Proceedings of the EC-TMR Conference held in Rome, Italy, October, 1998*, American Institute of Physics, vol. 476, ed by L. Maiani, F. Melchiorri, N. Vittorio (Woodbury, N.Y. 1999) pp 204 – 223
29. G. de Zotti, R. Ricci, D. Mesa, L. Silva, P. Mazzotta, L. Toffolatti, J. González-Nuevo: A&A, **431**, 893 (2005)
30. J. M. Diego, P. Vielva, E. Martínez-González, J. Silk, J.L. Sanz: MNRAS, **336**, 1351 (2002)
31. J. M. Diego, P. Vielva, E. Martínez-González, J. Silk: preprint (astro-ph/0403561)
32. H. Dole, G. Lagache, J.-L. Puget: ApJ, **585**, 617 (2003)
33. B. T. Draine, A. Lazarian: ApJ, **494**, L19 (1998)
34. B. T. Draine, A. Lazarian: ApJ, **508**, 157 (1998)
35. H. K. Eriksen, A. J. Banday, K. M. Górski, P. B. Lilje: ApJ, **612**, 633 (2004)
36. H. K. Eriksen et al.: ApJ, submitted (2005), preprint (astro-ph/0508268)
37. D. P. Finkbeiner, G. I. Langston, A. H. Minter: ApJ, **617**, 350 (2004)
38. O. Forni, N. Aghanim: A&A, **420**, 49 (2004)
39. J. González-Nuevo, L. Toffolatti, F. Argüeso: ApJ, **621**, 1 (2005)
40. G. L. Granato, G. de Zotti, L. Silva, A. Bressan, L. Danese: ApJ, **600**, 580 (2004)
41. B. Guiderdoni: Far-Infrared Point Sources. In: *Microwave Foregrounds*, ASP Conference Series, vol 181, ed by A. de Oliveira-Costa, M. Tegmark (1999), pp 173 – 198
42. M. G. Haehnelt & M Tegmark: MNRAS, **279**, 545 (1996)
43. D. Herranz, J.L. Sanz, M.P. Hobson, R.B. Barreiro, J.M. Diego, E. Martínez-González, A.N. Lasenby: MNRAS, **336**, 1057 (2002)
44. D. Herranz, J. Gallegos, J.L. Sanz, E. Martínez-González: MNRAS, **334**, 353 (2002)
45. D. Herranz, J.L. Sanz, R.B. Barreiro, E. Martínez-González: ApJ, **580**, 610 (2002)
46. D. Herranz: Analysis of the anisotropies in the Cosmic Microwave Background Radiation using Adaptive Filters. PhD Thesis, Universidad de Cantabria, Spain (2002)
47. D. Herranz, E. E. Kuruoglu, L. Toffolatti: A&A, **424**, 1081 (2004)

48. D. Herranz, J.L. Sanz, R.B. Barreiro, M. López-Caniego: MNRAS, **356**, 944 (2005)
49. M. P. Hobson, A. W. Jones, A. N. Lasenby, F. R. Bouchet: MNRAS, **300**, 1 (1998)
50. M. P. Hobson, R. B. Barreiro, L. Toffolatti, A. N. Lasenby, J. L. Sanz, A. W. Jones, F. R. Bouchet: MNRAS, **306**, 232 (1999)
51. M.P. Hobson, C. McLachlan: MNRAS, **338**, 765 (2003)
52. A. Kashlinsky, F. Atrio-Barandela: ApJ, **536**, 67 (2000)
53. K. K. Knudsen, V. E. Barnard, R. P. van der Werf, P. Vielva, J.-P. Kneib, A. W. Blain, R. B. Barreiro, R. J. Ivison, I. R. Smail, J. A. Peacock: MNRAS, submitted (2005)
54. E. Komatsu, D. N. Spergel: PhRvD, **63**, 063002 (2001)
55. E. Komatsu et al.: ApJS, **148**, 119 (2003)
56. G. Lagache: A&A, **405**, 813 (2003)
57. M. López-Caniego, D. Herranz, R. B. Barreiro, J. L. Sanz: SPIE, **5299**, 145 (2004)
58. M. López-Caniego, D. Herranz, R. B. Barreiro, J. L. Sanz: MNRAS, **359**, 993 (2005)
59. M. López-Caniego, D. Herranz, J. L. Sanz, R. B. Barreiro: EURASIP Journal on Applied Signal Processing (Special Issue on Applications of Signal Processing in Astrophysics and Cosmology), **15**, 1 (2005)
60. M. López-Caniego, J. L. Sanz, D. Herranz, J. González-Nuevo, R. B. Barreiro, E. E. Kuruoglu: *Non-linear fusion of images and the detection of point sources*. In: IEEE proceedings of the International Workshop on Nonlinear Signal and Image Processing, in press (2005)
61. M. López-Caniego, J. L. Sanz, D. Herranz, R. B. Barreiro, J. González-Nuevo: *Linear and quadratic fusion of images: detection of point sources*. In: Proceedings of the 13th European Signal Processing Conference (EUSIPCO 2005), in press (2005)
62. D. Maino, A. Farusi, C. Baccigalupi, F. Perrotta, A. J. Banday, L. Bedini, C. Burigana, G. de Zotti, K. M. Górska, E. Salerno: MNRAS, **334**, 53 (2002)
63. D. Maino, A. J. Banday, C. Baccigalupi, F. Perrotta, K. M. Górska: MNRAS, **344**, 544 (2003)
64. E. Martínez-González, J. E. Gallegos, F. Argüeso, L. Cayón, J. L. Sanz: MNRAS, **336**, 22 (2002)
65. E. Martínez-González, J. M. Diego, P. Vielva, J. Silk: MNRAS, **345**, 1101 (2003)
66. P. Mukherjee, B. Dennison, B. Ratra, J. H. Simonetti, K. Ganga, J.-C. Hamilton: ApJ, **579**, 83 (2002)
67. P. Naselsky, D. Novikov, J. Silk: MNRAS, **335**, 550 (2002)
68. G. Patanchon, J. F. Cardoso, J. Delabrouille, P. Vielva: MNRAS, in press (2005), preprint (astro-ph/0410280)
69. Planck Mission: <http://www.rssd.esa.int/Planck>
70. E. Pierpaoli: ApJ, **589**, 58 (2003)
71. E. Pierpaoli, S. Anthoine, K. Huffenberger, I. Daubechies: MNRAS, **359**, 261 (2005)
72. J. A. Rubiño-Martín, R. A. Sunyaev: MNRAS, **344**, 1155 (2003)
73. J. L. Sanz, D. Herranz & E. Martínez-González: ApJ, **552**, 484 (2001)
74. B. M. Schaefer, C. Pfrommer, R. Hell, M. Bartelmann: MNRAS, submitted, preprint (astro-ph/0407090)

75. A. E. Schulz & M. White: *ApJ*, **586**, 723 (2003)
76. V. Stolyarov, M. P. Hobson, M. A. J. Ashdown, A. N. Lasenby: *MNRAS*, **336**, 97 (2002)
77. V. Stolyarov, M. P. Hobson, A. N. Lasenby, R. B. Barreiro: *MNRAS*, **357**, 145 (2005)
78. R. A. Sunyaev, Ya. B. Zel'dovich: *Ap&SS*, **7**, 3 (1970)
79. R. A. Sunyaev, Ya. B. Zel'dovich: *CoASP*, **4**, 173 (1972)
80. R. A. Sunyaev, Ya. B. Zel'dovich: *MNRAS*, **190**, 413 (1980)
81. M. Tegmark & G. Efstathiou: *MNRAS*, **281**, 1297 (1996)
82. M. Tegmark, A. de Oliveira-Costa: *ApJ*, **500**, L83 (1998)
83. M. Tegmark, D. J. Eisenstein, W. Hu, A. de Oliveira-Costa: Overview of the foregrounds and their impact. In: *Microwave Foregrounds*, ASP Conference Series, vol 181, ed by A. de Oliveira-Costa, M. Tegmark (1999), pp 3 – 58
84. M. Tegmark, A. de Oliveira-Costa, A. J. S. Hamilton: *Phys. Rev. D.*, **68**, 123523 (2003)
85. L. Toffolatti, F. Argüeso-Gómez, G. De Zotti, P. Mazzei, A. Francheschini, L. Danese, C. Burigana: *MNRAS*, **297**, 117 (1998)
86. M. Tucci, E. Martínez-González, L. Toffolatti, J. González-Nuevo, G. De Zotti: *MNRAS*, **349**, 1267 (2004)
87. P. Vielva, E. Martínez-González, L. Cayón, J.L. Sanz, L. Toffolatti: *MNRAS*, **326**, 181 (2001)
88. P. Vielva, R.B. Barreiro, M.P. Hobson, E. Martínez-González, A.N. Lasenby, J.L. Sanz, L. Toffolatti: *MNRAS*, **328**, 1 (2001)
89. P. Vielva, E. Martínez-González, J.E. Gallegos, L. Toffolatti L., J.L. Sanz: *MNRAS*, **344**, 89 (2003)